Journal Pre-proof

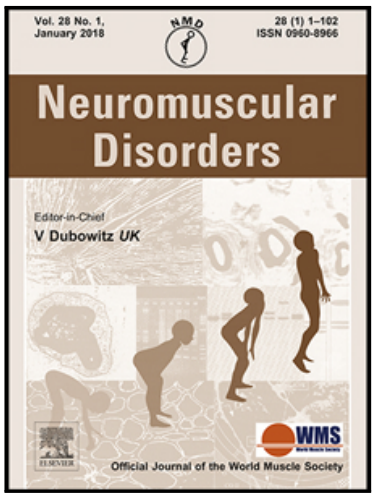

Whole-Body muscle MRI in McArdle disease

Tobaly David MD , Laforêt Pascal MD, PhD , Stojkovic Tanya MD , Behin Anthony MD , Petit Francois Michael PharmD, PhD , Barp Andrea MD , Bello Luca MD, PhD , Carlier Pierre MD, PhD , Carlier Robert-Yves MD

PII: S0960-8966(21)00584-8
DOI: https://doi.org/10.1016/j.nmd.2021.07.397
Reference: NMD 4042

To appear in: *Neuromuscular Disorders*

Received date: 15 June 2020
Revised date: 14 June 2021
Accepted date: 20 July 2021

Please cite this article as: Tobaly David MD , Laforêt Pascal MD, PhD , Stojkovic Tanya MD , Behin Anthony MD , Petit Francois Michael PharmD, PhD , Barp Andrea MD , Bello Luca MD, PhD , Carlier Pierre MD, PhD , Carlier Robert-Yves MD , Whole-Body muscle MRI in McArdle disease, *Neuromuscular Disorders* (2021), doi: https://doi.org/10.1016/j.nmd.2021.07.397

Whole-Body muscle MRI in McArdle disease

Tobaly David MD[1], Laforêt Pascal MD, PhD[1,2,3], Stojkovic Tanya MD[4], Behin Anthony MD[3], Petit Francois Michael PharmD, PhD[5], Barp Andrea MD[6], Bello Luca MD, PhD[6], Carlier Pierre MD, PhD[7], Carlier Robert-Yves MD [1,3,8].

[1] APHP, Service de Radiologie GH Université Paris-Saclay DMU Smart Imaging, Hôpital Raymond Poincaré, 104 boulevard Raymond Poincaré, Garches, France.

[2] AP-HP, Service de Neurologie, GH Université Paris-Saclay, DMU Neuro-Handicap, Hôpital Raymond-Poincaré, Garches, France

[3] Centre de référence des maladies neuromusculaires Nord/Est/Ile de France, France

[4] AP-HP, Hôpital Pitié-Salpêtrière, 75013, Paris, France.

[5] APHP, Laboratoire de Génétique Moléculaire, Université Paris Saclay, Hôpital Antoine Béclère, 92140 Clamart, France.

[6] Neurosciences Department (DNS), University of Padova, Padova, Italy

[7] AIM & CEA NMR Laboratory, Institute of Myology, Pitié-Salpêtrière University Hospital, Paris, France

[8] UMR 1179, Université Versailles Saint Quentin en Yvelines, Paris Saclay, France

Running head : WB-MRI IN McARDLE DISEASE

<u>The name of the corresponding author</u>

David Tobaly

Email : davtoba@gmail.com; Tel : +33667118814

Adresse : 7, rue Paul Cézanne, 94400, Vitry sur Seine

HIGHLIGHTS

- • Distribution of muscles involvement helps in directing the diagnosis towards a myopathy
- • The main relevant clinical data was the correlation between age and disease severity
- • A general symmetrical muscle alteration was noticed except for the subscapularis
- • Subscapularis, anterior serratus and quadratus femoris muscles were mainly involved

Whole-Body muscle MRI in McArdle disease

Introduction

This study describes muscle involvement on whole-body MRI (WB-MRI) scans at different stages of McArdle disease (MD).

Methods

WB-MRI was performed on fifteen genetically confirmed MD patients between ages 25 to 80. The degree of fatty substitution was scored for 60 muscles using Mercuri's classification.

Results

All patients reported an intolerance to exercise and episodes of rhabdomyolysis. A mild fixed muscle weakness was observed in 13/15 patients with neck flexor weakness in 7/15 cases, and proximal muscle weakness in 6/15 cases. A moderate scapular winging was observed in five patients.

A careful review of the MRI scans, as well as hierarchical clustering of patients by Mercuri scores, pointed out recurrent muscle changes particularly in the subscapularis, anterior serratus, erector spinae and quadratus femoris muscles.

Discussion

WB-MRI imaging provides clinically relevant information and is a useful tool to orient toward the diagnosis of MD.

I - Introduction

McArdle disease, also known as glycogen storage disease type V (GSD V), is the most common form of muscle glycogenosis [1]. It is caused by a deficiency of the myophosphorylase enzyme and is the result of an autosomal recessive mutation of the *PYGM* gene. Patients present typical clinical manifestations such as lifelong history of exercise intolerance and rhabdomyolysis episodes with onset in childhood. Moreover, approximately 35 % of the patients affected by McArdle disease also develop permanent muscle weakness between the ages of 40-50 [2,3].

An increasing number of studies demonstrate that MRI can be a powerful complementary tool for clinicians to identify muscle alterations and patterns of distribution in patients with permanent muscle weakness [4–6]. Its availability, rapidity of acquisition and valuable findings compared to CT place this modality as an optimal technique to assess skeletal muscle edema or fibroadipose tissue transformation. Moreover, MRI could also enable the detection of subtle and early muscle involvement in younger patients not showing clinical weakness [7]. Generally, an increase in T1 weighted (T1w) signal intensity suggests fat substitution into muscle, whereas decreased muscle volume suggests atrophy. A careful analysis of the distribution of the abnormalities within each of the different muscle groups is a critical factor in directing the diagnosis towards an underlying myopathy.

The development of Whole-Body MRI (WB-MRI) explorations has strengthened the assessment of these criteria by implementing new protocols such as Dixon fat fraction extraction and by including all the muscles in a single scan.

To the best of our knowledge, McArdle disease has never been systematically studied through a morphological mapping on WB-MRI despite the heterogeneity of the clinical manifestations which can lead to erroneous diagnosis [8,9]. Interestingly, only few case reports outlined this disease as a severe axial myopathy [10]. More recently, MRIs comprising a muscle diffusion

tensor imaging in McArdle patients didn't provide additional information to detect intracellular glycogen accumulation in muscle fibers [11]. Conversely, Carbon-13 magnetic resonance spectroscopy appears to be useful to quantify glycogen levels in muscle. However, its widespread utilization is limited due to technical limitations inherent to this technique [12]. Therefore, WB-MRI scans could be very helpful as a prolongation of the standard clinical examination, especially when it comes to evaluating the distribution of the affected muscles. Therefore, the pattern of affected muscles could reveal important information in the etiological analysis, as was determined in other myopathies and glycogenosis [13,14].

Thus, the main goal of this study is to depict a suggestive pattern of muscle involvement using whole-body muscle MRI in 15 patients with genetically confirmed McArdle disease.

II - Methods:

2.1 Patients

All patients included in this study had a biochemical and genetically proven diagnosis of GSDV as well as an available clinical record. They were also willing and capable of undergoing an MRI scan.

Muscle weakness was assessed using manual muscle testing and the Medical Research Council (MRC) score, a tool specifically developed to assess muscle strength in different conditions [15].

All clinical data were recorded, including the age of onset, presenting features, and muscle weakness. Non-eligibility criteria were incomplete WB-MRI scans.

The research ethics committee approved this study at our institution, and informed consent was obtained from all patients.

2.2 Molecular analysis

Genomic DNA was extracted from peripheral leukocytes. All the exons and intron/exons junctions of the PYGM gene were PCR-amplified and then sequenced using the same oligonucleotide primers. Sequences obtained were compared to the reference sequence NM_005609.4.

2.3 Muscle imaging

Most of the patients underwent whole-body imaging on a free-bore 3T General Electric (GE) Discovery MR750w GEM system (General Electric, Boston, MA, USA) or on a 3T Siemens MAGNETOM Avanto system (Siemens, Magnetom Trio TIM, Erlangen, Germany). Both systems employ multiple phased-array surface receiver elements. In the whole-body configuration, the patient was wrapped in a multi-coil and multi-element network. The patient's head and face muscles were imaged by a head coil usually intended for the brain. The setup enabled a maximum combined field of view (FOV) of 180 to 200 cm in order to have a whole-body scan in all patients.

For each orientation (coronal then axial), data acquisition was completed in five to seven steps during the patient's head-first passage through the magnet. In the coronal orientation, the images acquired successively at a same slice level were automatically combined to generate a single coronal composite view using the constructor's optional software. No manual realignment was needed.

On the Siemens platform, the selected imaging sequences were T1-weighted turbo spin-echo according to the recommended parameters for whole-body muscle imaging in diagnosis and outcome measures of neuromuscular disorders [6].

On the General Electric platform, the selected imaging sequences were 3D T1-weighted imaging in the coronal plane with a multi-stack exploration of the body from head to mid-thigh. Then, a fat-water separation protocol presented by GE (IDEAL T2; GE, Milwaukee, Wis) with a bespoke reconstruction algorithm based on a 3 points DIXON technique was used in the axial plane with multi-stack exploration from head to toe. This technique consists of the iterative decomposition of water and fat with echo asymmetry and least-squares estimation [16,17].

Water, as well as fat images and in and out phase images, were available for each slice, and the recommended parameters were followed in terms of spatial resolution.
To reduce acquisition time, “IDEAL T2” by General Electric (GE) protocols have been developed with in-out T2 weighted sequences within the same image sequence in the same stack, with fat and water images comparable to STIR sequences with better resolution.
The maximal 500 mm FOV was large enough to scan all patients. The technique required patient positioning with upper limbs lying close along or above the body.
No paramagnetic contrast agent was injected. No cardiac or respiratory gating was performed.
A multibreath-hold option was added to the thoracic sequence steps in patients who could hold their breath. Whole-body scanning was performed in a short time by using MRI software.

2.4 Data analysis

A visual qualitative four-point grading scale evaluated by a senior specialized radiologist allowed the assessment of quality screening (1: inadequate, 2: suboptimal, 3: good, 4: excellent).
Muscle analysis consisted of the examination of 60 paired muscles including the tongue.

Muscles were systematically explored using multi-stacks from head to toe in both axial and coronal slices encompassing the entire volume. Scoring was performed on the whole volume of each muscle.

Eight anatomical regions were then defined: face, neck, shoulder girdle, arms, and forearms, upper and lower trunk, pelvic girdle, thighs, and legs.

As axial muscles were of particular interest in our study, a careful analysis was also aimed at distinguishing the impairment of the transversospinalis and the erector spinae.

The transversospinalis include the deep intrinsic back muscles and consist of the semispinalis, multifidus, and rotatores. The erector spinae include the three intermediate back muscles and consists of the iliocostalis, longissimus, and spinalis [18,19].

These muscles were individualized on the Mercuri report.

For each patient, a median value of the extent of T1w hyperintensity was scored from 1 (normal) to 4 (end-stage disease) according to Mercuri's classification to assess fatty substitution as previously described [20].

- 1 = normal
- 2 = fat replacement less than 30%
- 3 = fat replacement ratio estimated between 30% and 60%
- 4 = fat replacement in muscle is greater than 60%

Then, a total mean score was calculated to determine the average value of the Mercuri's classification for every single muscle throughout our population.

For the axial images acquired on the GE platform using IDEAL T2 sequence, the fat images were analyzed instead of the T1 weighted images acquired with the Siemens platform.

For T2 fat-saturated weighted images (water images of the IDEAL T2 axial sequence) of the WB MRI obtained on the GE platform, the edema pattern of abnormal muscle signal intensity was increased and superimposed on an otherwise normal appearance of the involved muscle. Heatmaps were drawn with the "Fantastic Heatmap" package for R (package version 1.0.1, R version 3.5.3). Abnormal findings in the whole-body examination were recorded for bone and joint as well as chest and abdomen.

3. Results

3.1 Clinical evaluation

Fifteen patients (eleven male and four female) aged 24 to 84 years (mean 49.3 years) completed the study. Most patients were diagnosed in adulthood despite having reported exercise intolerance and myoglobinuria episodes since their childhood. At the time of this study, fixed muscle weakness was observed at the clinical examination in 13 patients (*table 1*).

3.2 Imaging findings

Whole-body muscle imaging was possible for all patients.

Images obtained for most of the exams were graded as excellent. None were classified as inadequate. Three types of artifacts decreased the quality of MRI scans; motion artifacts, respiratory artifacts (which affect only thoracic and abdominal images), and phase wrap-around artifacts as a manifestation of the aliasing phenomenon (on the shoulder and upper arms). Scanning time was less than 35 min. In-room time ranged from 40 to 50 min with a mean time of 43 min.

Muscle changes seen in T1w sequences consisted mostly of fat replacement, which manifests itself as a bright signal, but without severe muscle atrophy (i.e., muscle shape and volume

were preserved although the inner content changed). Schematic representations of mean MRI muscle scoring in the upper and lower part of the body are represented below (fig 1).

Fatty substitution was slightly asymmetric for the subscapularis muscle (half point of the Mercuri scale). Otherwise, an overall symmetric involvement was identified in other muscles, as described below.

The heatmap of fibro-fatty substitution scores (fig 2) showed a distal-to-proximal gradient of mild-to-severe muscle involvement with most marked alterations in axial muscles.

The length of the two main branches of the dendogram obtained by unsupervised hierarchical clustering of participants means that a dichotomy was observed, rather than a continuum, in the degree of muscle fatty replacement in patients 5, 12, and 14. These patients are all over 45 years old, indicating a correlation of muscle fatty replacement with age, where older patients tend to be more affected.

3.2.1 Upper part of the body

Most facial muscles, including the tongue, were systematically spared without any significant fatty modification.

In the shoulder girdle, the most prominent involvement was located on the subscapularis muscles with a slight mean predominance on the left side. It was followed by symmetric substitution of the anterior serratus and the trapezius (fig 3).

No abnormality was described for anterior and posterior compartments of arms and forearms.

3.2.2 Lower part of the body

Pelvis and thigh involvement was present only in patients with the most severe muscle involvement in MRI (fig 2). Therefore, lower body involvements on MRI appears to be

related to advanced disease. Muscle changes were dominated by alterations on the quadratus femoris and adductor longus muscles with a mean score on MRI of 1.73 and 1.20 respectively (fig 1).

Otherwise, all the other muscles of this region remained relatively intact (fig 4).

Leg changes were homogeneous and remarkably faint, particularly in the soleus muscles (mean score of 1.2).

3.2.3 Axial muscles

The transversospinalis muscles demonstrated a predominant involvement of the rotators and semispinalis with a mean score on MRI of 1.8 and 1.73 respectively, while the multifidus was slightly spared (mean score of 1.6).

The erector spinae muscles, including the spinalis, longissimus thoracis and iliocostalis muscles presented marked atrophy to such an extent (1.6 and 1.7 respectively) that their fasciae were retracted (fig 5). However, the iliopsoas, quadratus lumborum, and interspinous muscles were completely spared.

No high signal compatible with inflammatory changes or intramuscular edema was noticed on T2 fat saturated weighted images.

4. Discussion

This study aimed to describe the radiological pattern of muscle involvement based on a WB-MRI analysis in fifteen adults affected by GSDV. The main relevant clinical data was the correlation between age and disease severity [21]. No apparent correlation was observed between the incidence of fixed muscle weakness and genotype. This finding strengthens the hypothesis that severity of the disease is not solely explained through the genotype. There are many other factors that have not yet been fully identified but that can also potentially explain

impact on the genotype-phenotype correlation. Patient's gender may contribute to the clinical heterogeneity with women being more severely affected than men [22,23]. This difference could be explained by a maladaptive pain-related coping system predominant in women [22] . However, only four women were included in our study without revealing a significant clinical difference with the male patients.

Several environmental expositions and dietetic management seem to be essential point to consider in the heterogeneity of the disease manifestation.

Muscle Residual myophosphorylase activity was not assessed, being irrelevant for the diagnosis, knowing the pathogenicity of detected variants after molecular analysis. Moreover previous studies showed that quite all patients with McArdle disease don't have any residual myophosphorylase activity [24,25].

On WB-MRI, the findings of this study seem to indicate that most patients with GSDV have a pattern of muscle involvement that can help orient the clinician towards GSDV diagnosis; an almost perfectly symmetrical presentation throughout the whole-body along with a noticeable asymmetrical alteration of the scapular girdle, particularly in the subscapularis muscle. This asymmetric distribution in the scapular girdle remains, for now, unexplained. This is consistent with the results obtained by Nadaj-Pakleza et al. [2] who clinically evaluated the motor function of the scapular girdle. As this radiological presentation can also suggest FSHD, both must be considered in the differential diagnosis [2,26]. However, the clinical presentation differs greatly between the two disorders, and T2 signal alterations are more common in FSHD.

Another finding consisted of the damage caused to the axial muscles and more specifically to the thoracic extensor muscles. The latter is part of the paravertebral muscles whose primary function is to stabilize the spinal armature while participating in specific movements [15]. Medially to laterally, a mostly homogeneous and symmetrical fatty substitution as well as a

degeneration of erector spinae and transversospinalis muscles was observed. Nevertheless, it is interesting to note the slightly predominant damage in the erector spinae over the rotator muscles. This kind of muscle damage is consistent with and could explain a bent posture in GSDV patients [10].

Osteoarthritis, a highly prevalent disorder especially in the elderly population, is another potential differential diagnosis due to its involvement of the paravertebral muscles. In contrast with osteoarthritis, patients in this study did not present any degenerative reshaping of the spine. In addition, few studies have shown that the atrophy of the paravertebral muscles electively affects the multifidus conversely to the results obtained in this study.

Quinlivan et al. described axial impairment in 30% of their patients with McArdle disease [27] . Through the widespread use of MRI, more and more studies show a significant involvement of the axial musculature in several myopathies [28].

McArdle, Cori and Pompe are three major glycogenosis diseases with marked predominant axial involvement. In imaging, they share several commonalities. For example, McArdle and Pompe diseases present an extensive involvement of the axial musculature, more precisely in the subscapular and anterior serratus muscles. However, in McArdle disease, the tongue, the psoas, and the quadratus lumborum muscles are constantly spared. This pattern contrasts with the proven involvement of these muscles in Pompe disease [20] . Moreover, there are certain key factors that allow clinicians to differentiate between either disease, such as more severe muscle weakness in Pompe disease.

Another myopathy due to mutations in the lamin A/C gene is known for its predominant axial involvement [29].

Other myopathies such as calpainopathy [30], LGMD2D [31], dysferlinopathy [32] or those induced by mutations such as MATR3, could be included in the differential but the spectrum of axial manifestations is relegated. As a matter of fact, a study demonstrated that

calpainopathy [30] involved mainly the hip adductors and hamstrings in lower limbs compared to spine extensors and spine rotators . This is another distinguishing characteristic to differentiate McArdle disease from other axial myopathies including FSHD1. Indeed, in the latter there is an isolate subscapular involvement whereas the lower limbs are relatively spared, except the rectus femori [33].

Considering other diseases with camptocormia and abnormal posture can rapidly widen the differential. For example, even if Parkinson disease patients have cerebellar ataxia or autonomic symptoms, they have also fatty involution extended to the thoracolumbar spine musculature which appeared to be specific to the disease itself [34]. Therefore, the imaging findings in WB-MRI should always be guided by the whole clinical context.

Other metabolic myopathies with exercise intolerance such as glycogenosis type VII could expand the differential diagnosis despite the absence of imaging studies [35]. However, in a clinical setting, the apparent distinction between the two is simply made by the absence of the second wind phenomenon and the detrimental ("out of wind") response to glucose administration.

Furthermore, none of the patients suffered from scoliosis, which is a common feature in FSHD1 and collagen VI-related which are both considered to be asymmetrical myopathies.

In terms of facial involvement none were described despite reports in previous cases [36,37].

In the pelvic girdle, the quadratus femoris muscles presented an elective and strikingly asymmetrical involvement. The quadratus femoris originates on the lateral border of the ischial tuberosity and on the intertrochanteric crest of femur. It stabilizes the hip and acts as an external rotator. Its involvement was not described in any previous research, and it is not usually found in other myopathies. Meanwhile, it is also interesting to note that all the pelvic musculature was systematically spared. This visual contrast supports this finding that appears to be a highly suggestive parameter towards the diagnosis of McArdle's disease (fig. 6) [38].

Additionally, as part of the usual exploration protocol of myopathies in many centers, restricted analysis to the lower limbs could be truly insufficient. Conversely, the increasing discovery of fatty substitution of muscles without any obvious clinical expression emphasizes the need to perform exhaustive WB-MRI scans.

The WB-MRI analysis confirmed that all the patients did not have any muscle atrophy, but only fatty substitution as observed in other metabolic myopathies. However, this statement should be taken cautiously because there is no gold standard to evaluate muscle atrophy in WB-MRI.

Through a clinical lens, it is interesting to note that the clinico-radiological correlation presented a few inconsistencies. On one hand, three out of the four patients with scapular winging did not have any involvement of the serratus anterior. Furthermore, although clinical examination showed deltoid muscle and neck flexor weaknesses, they were spared in imaging in almost all patients. On the other hand, the clinical assessment did not raise concern about the impairment of the quadratus femori despite the clear involvement of this muscle in imaging.

This paradox reinforces the idea that clinical testing could often attribute inaccurate functional disability to a specific muscle whereas such testing is rather descriptive of the overall motor behavior of a group of synergistic muscles. Furthermore, clinical evaluation can be challenging due to the complex compartmental anatomy and several anatomical variations in muscle, such as the external rotator of the hip including the quadratus femori [39–41].

Although imaging can help facilitate the diagnostic approach, there are some limitations to be considered. Firstly, due to technical limitations, this study was unable to complete an analysis of the arms and forearms, which may have shown interesting anomalies as demonstrated in a previous clinical study [2].

Secondly, the specificity of imaging findings presents a limitation. At times, MRI can be overly sensitive and describe muscular alterations that have no substantial clinical impact. In fact, a clear clinical-imaging correlation could not be established in this study, even when there is a marked muscle alteration particularly in older patients. Still, the complex clinical and radiological layout of our cohort reinforces the inability to predict to what extent the underlying mutation contributes to the phenotype. Therefore, as found in most MRI studies on myopathies, several patients (c.f. patient 12 in our study) had marked MRI damage but this did not translate clinically. This finding is not unique to our series, but a limit found in most MRI studies on myopathies. As explained earlier, a potential explanation may be the integrity of the rest of the associated muscle group contributing to preserve the movement of the limb. Thirdly, all groups of muscle were not systematically examined clinically, neck flexors in particular. This limitation can illustrate the downside of the clinical examination, subject to less standardization and reproducibility. Therefore, an exhaustive and complementary imaging consistently brought by WB-MRI is genuinely valuable.

Also, the radiologist was not blinded to the condition.

Lastly, there was only fifteen patients included in our study. Even if this is a relative rare disease, the raising awareness of the benefit in performing WB-MRI in those patients will significantly improve the collaboration between research centers in order to establish larger cohorts.

In conclusion, WB-MRI enhances the diagnostic algorithm of muscle glycogenoses. Along with a careful review of the MRI scans, McArdle disease should be considered when there are muscle changes in the subscapularis, anterior serratus, erector spinae, and quadratus femoris muscles. Therefore, this study has value in showing the unique pattern of MD on WB-MRI,

and identifying "sentinel" muscles of potential interest for future longitudinal imaging studies.

FIGURE LEGENDS

Fig 1 - Schematic representation of mean MRI muscle scoring in the whole body (e.g.: the mean score for temporal muscle is 1 for the entire population indicating that this muscle is always preserved in this study).

Fig 2 - Hierarchically clustered heatmap of fatty substitution Mercuri scores in 60 muscles, in MRIs from 15 McArdle individuals. Rows, each corresponding to one individual, are hierarchically clustered (dendogram on the left) based solely on MRI data (Mercuri scores). Each column in the heatmap corresponds to one muscle, ordered left to right from cranial to caudal. A green-yellow-red gradient in the heatmap indicates increasing fatty substitution (legend to the right). The column left of the heatmap annotates individual clinical/demographic features (not used in the hierarchical clustering algorithm): probability of myophosphorylase residual activitiy predicted by the patient's genetic mutations, Medical Research Council (MRC) lowest score, and age.

Fig 3 - Axial fat image of the DIXON technique sections at the upper part of the body level in one McArdle patient. The right horizontal segment of the trapezius muscle (T) was affected (Fig 3A). The predominant muscle involved in the scapular girdle was the subscapularis muscle (SC) as shown bilaterally here (Fig 3B). Another finding was alteration on anterior serratus muscle (AS) with partial views of the arms (Fig 3C).

Fig 4 - Axial fat image of the DIXON technique sections at the lower part of the body level in one McArdle patient. Asymmetrical involvement of the left adductor longus (LA) and the right quadratus femoris (QF).

Fig 5 – Axial and coronal fat image of the DIXON technique sections exploring the paravertebral muscles in one McArdle patient. The transversopinalis muscles demonstrated a predominant involvement on the rotators (R) and semi-spinalis (non

represented) while the multifidus (M) were slightly spared (Fig 5A). The erector spinae muscles including spinalis, longissimus thoracis (L) and iliocostalis muscles (IC) presented an overall marked alteration to such an extent that their fascia (thin arrows) were retracted (Fig 5B). On the opposite, there was a clear sparing of the psoas (P), quadratus lumborum (QL) and interspinous muscles (bold arrow).

Fig 6 – Axial fat image of the DIXON technique sections exploring the different stages of findings in different disease stages of McArdle patients. The first one showed mild involvement, the second is more involved with fatty substitution of both quadratus femori, and the last one is more advanced with changing in the right quadratus femori and in the calf.

ABBREVIATIONS

WB-MRI : Whole-Body MRI

GSDV : glycogen storage disease type V

MD : McArdle Disease

GE : General Electric

FOV : field of view

FSHD : fascioscapulohumeral muscular dystrophy

REFERENCES

[1] De Castro M, Johnston J, Biesecker L. Determining the prevalence of McArdle disease from gene frequency by analysis of next-generation sequencing data. Genet Med Off J Am Coll Med Genet 2015;17:1002–6. https://doi.org/10.1038/gim.2015.9.
[2] Nadaj-Pakleza AA, Vincitorio CM, Laforêt P, Eymard B, Dion E, Teijeira S, et al. Permanent muscle weakness in McArdle disease. Muscle Nerve 2009;40:350–7. https://doi.org/10.1002/mus.21351.
[3] Lucia A, Nogales-Gadea G, Pérez M, Martín MA, Andreu AL, Arenas J. McArdle disease: what do neurologists need to know? Nat Clin Pract Neurol 2008;4:568–77. https://doi.org/10.1038/ncpneuro0913.
[4] Warman Chardon J, Díaz-Manera J, Tasca G, Bönnemann CG, Gómez-Andrés D, Heerschap A, et al. MYO-MRI diagnostic protocols in genetic myopathies. Neuromuscul Disord NMD 2019;29:827–41. https://doi.org/10.1016/j.nmd.2019.08.011.
[5] Jungbluth H. Myopathology in times of modern imaging. Neuropathol Appl Neurobiol 2017;43:24–43. https://doi.org/10.1111/nan.12385.

[6] Leung DG. Magnetic resonance imaging patterns of muscle involvement in genetic muscle diseases: a systematic review. J Neurol 2017;264:1320–33. https://doi.org/10.1007/s00415-016-8350-6.
[7] Mercuri E, Pichiecchio A, Allsop J, Messina S, Pane M, Muntoni F. Muscle MRI in inherited neuromuscular disorders: past, present, and future. J Magn Reson Imaging JMRI 2007;25:433–40. https://doi.org/10.1002/jmri.20804.
[8] Pallo PAO, Silva AMS da, Zanoteli E, Shinjo S. McArdle's disease: an underestimated or underdiagnosed myopathy in rheumatologic practice? Cases series and literature review. MedicalExpress 2018;5. https://doi.org/10.5935/medicalexpress.2018.mo.008.
[9] Leite A, Oliveira N, Rocha M. McArdle disease: a case report and review. Int Med Case Rep J 2012;5:1–4. https://doi.org/10.2147/IMCRJ.S28664.
[10] Witting N, Duno M, Piraud M, Vissing J. Severe axial myopathy in McArdle disease. JAMA Neurol 2014;71:88–90. https://doi.org/10.1001/jamaneurol.2013.3209.
[11] Rehmann R, Schlaffke L, Froeling M, Kley RA, Kühnle E, De Marées M, et al. Muscle diffusion tensor imaging in glycogen storage disease V (McArdle disease). Eur Radiol 2019;29:3224–32. https://doi.org/10.1007/s00330-018-5885-1.
[12] Heinicke K, Dimitrov IE, Romain N, Cheshkov S, Ren J, Malloy CR, et al. Reproducibility and absolute quantification of muscle glycogen in patients with glycogen storage disease by 13C NMR spectroscopy at 7 Tesla. PloS One 2014;9:e108706. https://doi.org/10.1371/journal.pone.0108706.
[13] Díaz-Manera J, Alejaldre A, González L, Olivé M, Gómez-Andrés D, Muelas N, et al. Muscle imaging in muscle dystrophies produced by mutations in the EMD and LMNA genes. Neuromuscul Disord NMD 2016;26:33–40. https://doi.org/10.1016/j.nmd.2015.10.001.
[14] Gómez-Andrés D, Dabaj I, Mompoint D, Hankiewicz K, Azzi V, Ioos C, et al. Pediatric laminopathies: Whole-body magnetic resonance imaging fingerprint and comparison with Sepn1 myopathy. Muscle Nerve 2016;54:192–202. https://doi.org/10.1002/mus.25018.
[15] Aids to the investigation of peripheral nerve injuries. Medical Research Council: Nerve Injuries Research Committee. His Majesty's Stationery Office: 1942; pp. 48 (iii) and 74 figures and 7 diagrams; with aids to the examination of the peripheral nervous system. By Michael O'Brien for the Guarantors of Brain. Saunders Elsevier: 2010; pp. [8] 64 and 94 Figures - PubMed n.d. https://pubmed.ncbi.nlm.nih.gov/20928945/ (accessed February 19, 2021).
[16] Reeder SB, Wen Z, Yu H, Pineda AR, Gold GE, Markl M, et al. Multicoil Dixon chemical species separation with an iterative least-squares estimation method. Magn Reson Med 2004;51:35–45. https://doi.org/10.1002/mrm.10675.
[17] Reeder SB, Pineda AR, Wen Z, Shimakawa A, Yu H, Brittain JH, et al. Iterative decomposition of water and fat with echo asymmetry and least-squares estimation (IDEAL): application with fast spin-echo imaging. Magn Reson Med 2005;54:636–44. https://doi.org/10.1002/mrm.20624.
[18] Bustami FM. A new description of the lumbar erector spinae muscle in man. J Anat 1986;144:81–91.
[19] Creze M, Soubeyrand M, Gagey O. The paraspinal muscle-tendon system: Its paradoxical anatomy. PLOS ONE 2019;14:e0214812. https://doi.org/10.1371/journal.pone.0214812.
[20] Carlier R-Y, Laforet P, Wary C, Mompoint D, Laloui K, Pellegrini N, et al. Whole-body muscle MRI in 20 patients suffering from late onset Pompe disease: Involvement patterns. Neuromuscul Disord NMD 2011;21:791–9. https://doi.org/10.1016/j.nmd.2011.06.748.

[21] Amato AA. Sweet success--a treatment for McArdle's disease. N Engl J Med 2003;349:2481–2. https://doi.org/10.1056/NEJMp038183.
[22] Rommel O, Kley RA, Dekomien G, Epplen JT, Vorgerd M, Hasenbring M. Muscle pain in myophosphorylase deficiency (McArdle's disease): the role of gender, genotype, and pain-related coping. Pain 2006;124:295–304. https://doi.org/10.1016/j.pain.2006.04.017.
[23] Rubio JC, Gómez-Gallego F, Santiago C, García-Consuegra I, Pérez M, Barriopedro MI, et al. Genotype modulators of clinical severity in McArdle disease. Neurosci Lett 2007;422:217–22. https://doi.org/10.1016/j.neulet.2007.06.025.
[24] Nogales-Gadea G, Brull A, Santalla A, Andreu AL, Arenas J, Martín MA, et al. McArdle Disease: Update of Reported Mutations and Polymorphisms in the PYGM Gene. Hum Mutat 2015;36:669–78. https://doi.org/10.1002/humu.22806.
[25] Nogales-Gadea G, Rubio JC, Fernandez-Cadenas I, Garcia-Consuegra I, Lucia A, Cabello A, et al. Expression of the muscle glycogen phosphorylase gene in patients with McArdle disease: the role of nonsense-mediated mRNA decay. Hum Mutat 2008;29:277–83. https://doi.org/10.1002/humu.20649.
[26] Bhavaraju-Sanka R, Jr JH, Chahin N. Atypical McArdle's disease with asymmetric weakness and Atrophy. SOJ Neurol 2014;1.
[27] Quinlivan R, Buckley J, James M, Twist A, Ball S, Duno M, et al. McArdle disease: a clinical review. J Neurol Neurosurg Psychiatry 2010;81:1182–8. https://doi.org/10.1136/jnnp.2009.195040.
[28] Witting N, Andersen LK, Vissing J. Axial myopathy: an overlooked feature of muscle diseases. Brain J Neurol 2016;139:13–22. https://doi.org/10.1093/brain/awv332.
[29] Maggi L, D'Amico A, Pini A, Sivo S, Pane M, Ricci G, et al. LMNA-associated myopathies: the Italian experience in a large cohort of patients. Neurology 2014;83:1634–44. https://doi.org/10.1212/WNL.0000000000000934.
[30] Liewluck T, Goodman BP. Late-onset axial myopathy and camptocormia in a calpainopathy carrier. J Clin Neuromuscul Dis 2012;13:209–13. https://doi.org/10.1097/CND.0b013e3182461a9c.
[31] Nguyen K, Bassez G, Krahn M, Bernard R, Laforêt P, Labelle V, et al. Phenotypic study in 40 patients with dysferlin gene mutations: high frequency of atypical phenotypes. Arch Neurol 2007;64:1176–82. https://doi.org/10.1001/archneur.64.8.1176.
[32] Kesper K, Kornblum C, Reimann J, Lutterbey G, Schröder R, Wattjes MP. Pattern of skeletal muscle involvement in primary dysferlinopathies: a whole-body 3.0-T magnetic resonance imaging study. Acta Neurol Scand 2009;120:111–8. https://doi.org/10.1111/j.1600-0404.2008.01129.x.
[33] Diaz-Manera J, Fernandez-Torron R, LLauger J, James MK, Mayhew A, Smith FE, et al. Muscle MRI in patients with dysferlinopathy: pattern recognition and implications for clinical trials. J Neurol Neurosurg Psychiatry 2018;89:1071–81. https://doi.org/10.1136/jnnp-2017-317488.
[34] Ohana M, Durand M-C, Marty C, Lazareth J-P, Maisonobe T, Mompoint D, et al. Whole-body muscle MRI to detect myopathies in non-extrapyramidal bent spine syndrome. Skeletal Radiol 2014;43. https://doi.org/10.1007/s00256-014-1909-3.
[35] Berardo A, DiMauro S, Hirano M. A diagnostic algorithm for metabolic myopathies. Curr Neurol Neurosci Rep 2010;10:118–26. https://doi.org/10.1007/s11910-010-0096-4.
[36] Pourmand R, Sanders DB, Corwin HM. Late-onset Mcardle's disease with unusual electromyographic findings. Arch Neurol 1983;40:374–7. https://doi.org/10.1001/archneur.1983.04050060074014.
[37] Hewlett RH, Gardner-Thorpe C. McArdle's disease--what limit to the age of onset? South Afr Med J Suid-Afr Tydskr Vir Geneeskd 1978;53:60–3.

[38] Kassarjian A, Tomas X, Cerezal L, Canga A, Llopis E. MRI of the quadratus femoris muscle: anatomic considerations and pathologic lesions. AJR Am J Roentgenol 2011;197:170–4. https://doi.org/10.2214/AJR.10.5898.
[39] Theodorou DJ, Theodorou SJ, Kakitsubata Y. Skeletal muscle disease: patterns of MRI appearances. Br J Radiol 2012;85:e1298–308. https://doi.org/10.1259/bjr/14063641.
[40] Robinson G, Hine AL, Richards PJ, Heron CW. MRI abnormalities of the external rotator muscles of the hip. Clin Radiol 2005;60:401–6. https://doi.org/10.1016/j.crad.2004.06.031.
[41] Sookhoo S, Mackinnon I, Bushby K, Chinnery PF, Birchall D. MRI for the demonstration of subclinical muscle involvement in muscular dystrophy. Clin Radiol 2007;62:160–5. https://doi.org/10.1016/j.crad.2006.08.012.

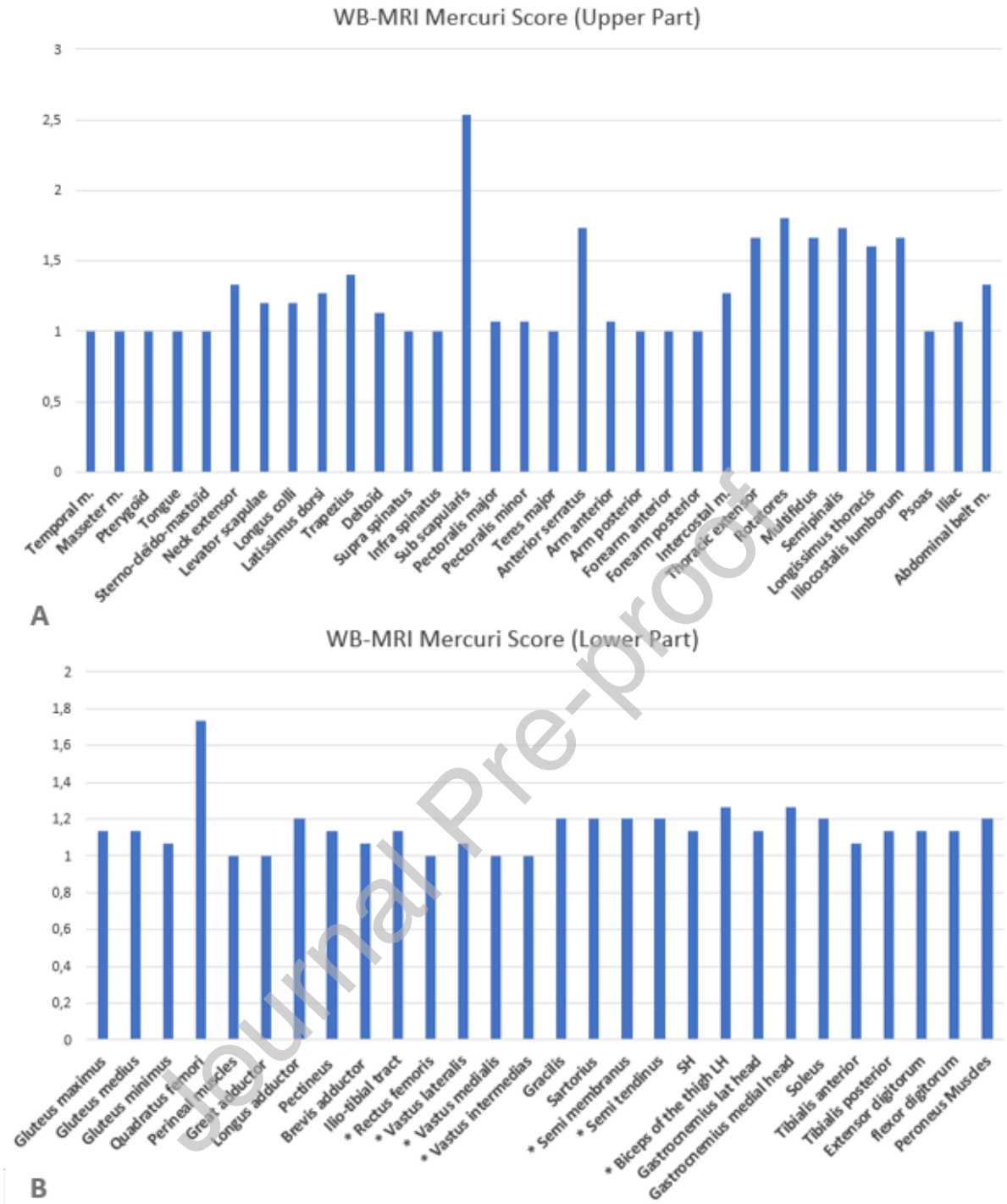

Fig 1 - Schematic representation of median WB-MRI scoring in 60 muscles in the upper part (A) and the low part (B) (e.g.: the mean score for temporal muscle is 1 for the entire population indicating that this muscle is always preserved in this study).

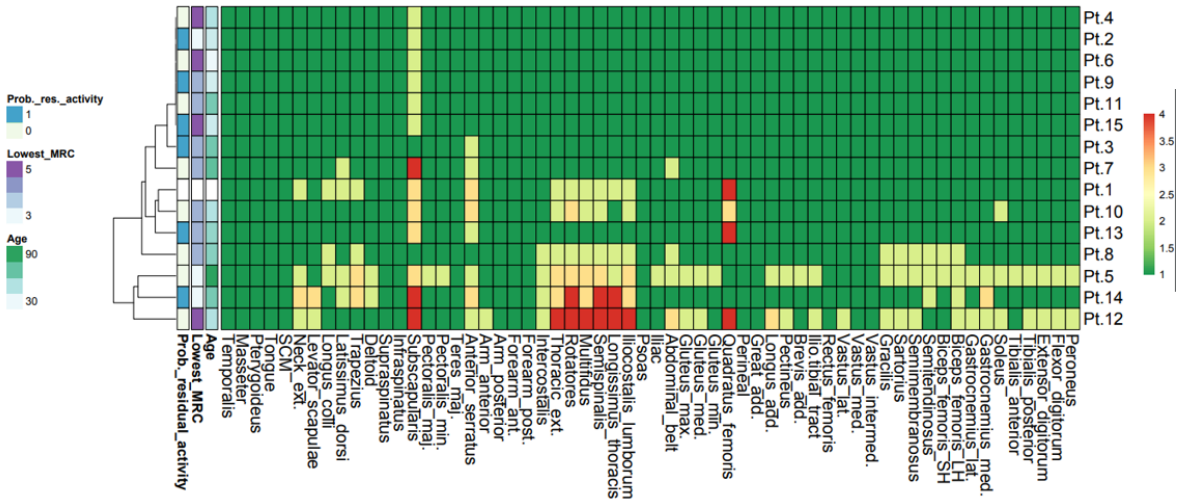

Fig 2 - Hierarchically clustered heatmap of fatty substitution Mercuri scores in 60 muscles, in MRIs from 15 McArdle individuals. Rows, each corresponding to one individual, are hierarchically clustered (dendogram on the left) based solely on MRI data (Mercuri scores). Each column in the heatmap corresponds to one muscle, ordered left to right from cranial to caudal. A green-yellow-red gradient in the heatmap indicates increasing fatty substitution (legend to the right). The column left of the heatmap annotates individual clinical features (not used in the hierarchical clustering algorithm): Medical Research Council (MRC).

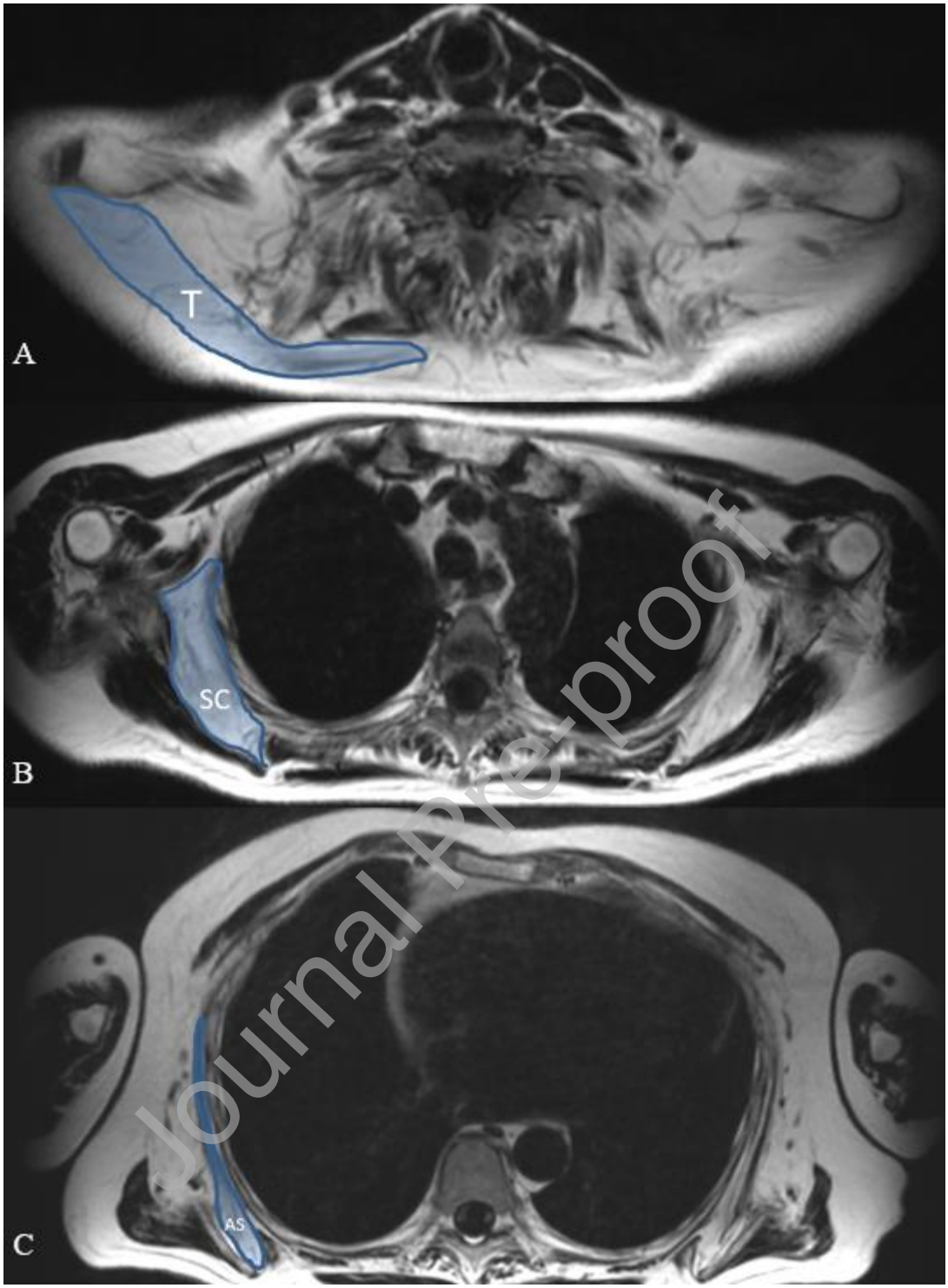

Fig 3 - **Axial fat image of the DIXON technique sections at the upper part of the body level in one McArdle patient.**
The right horizontal segment of the trapezius muscle (T) was affected (Fig 3A). The predominant muscle involved in the scapular girdle was the subscapularis muscle (SC) as shown bilaterally here (Fig 3B). Another finding was alteration on anterior serratus muscle (AS) with partial views of the arms (Fig 3C).

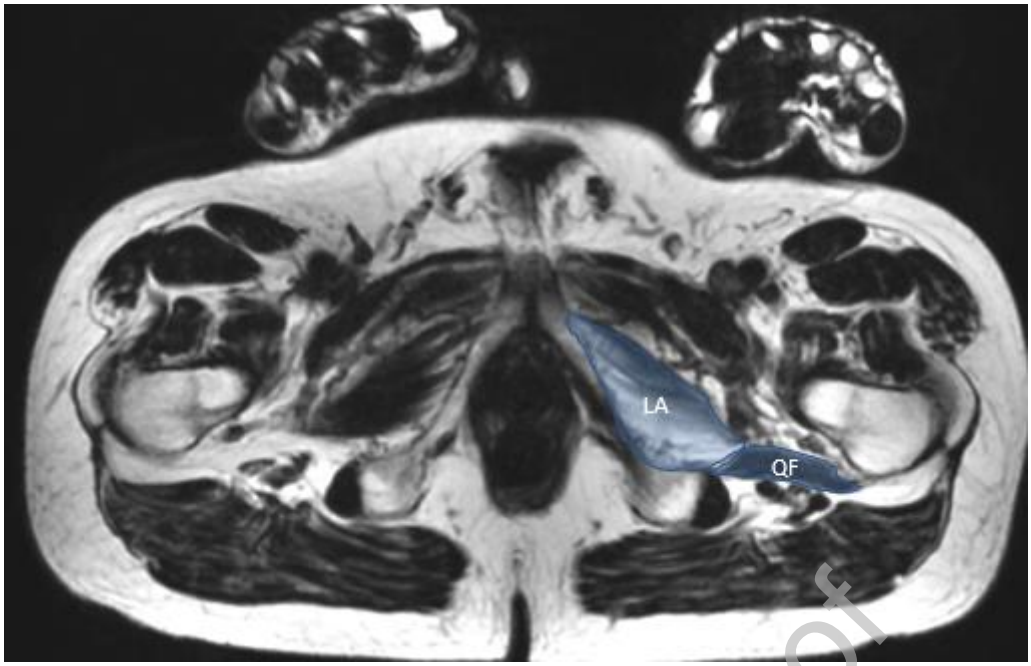

Fig 4 - Axial fat image of the DIXON technique sections at the lower part of the body level in one McArdle patient.
Asymmetrical involvement of the left longus adductor (LA) and the right quadratus femoris (QF).

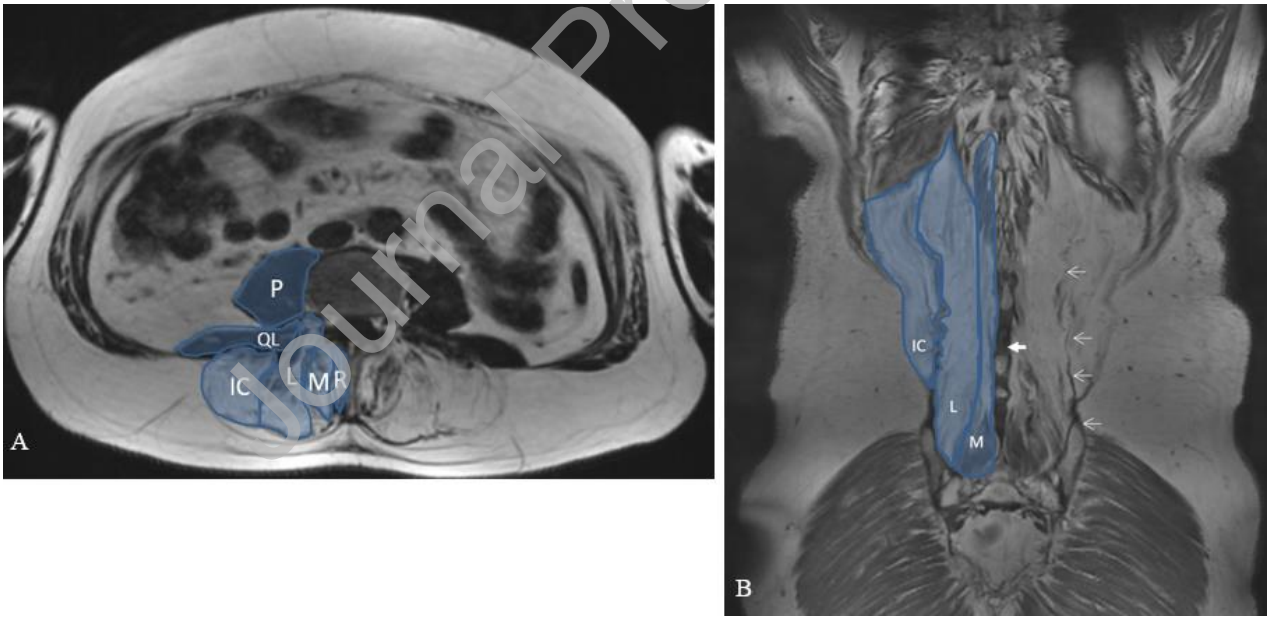

Fig 5 – Axial and coronal fat image of the DIXON technique sections exploring the paravertebral muscles in one McArdle patient.
The transversopinalis muscles demonstrated a predominant involvement on the rotators (R) and semi-spinalis (non represented) while the multifidus (M) were slightly spared (Fig 5A). The erector spinae muscles including spinalis, longissimus thoracis (L) and iliocostalis muscles (IC) presented an overall marked alteration to such an extent that their fascia (thin

arrows) were retracted (Fig 5B). On the opposite, there was a clear sparing of the psoas (P), quadratus lumborum (QL) and interspinous muscles (bold arrow).

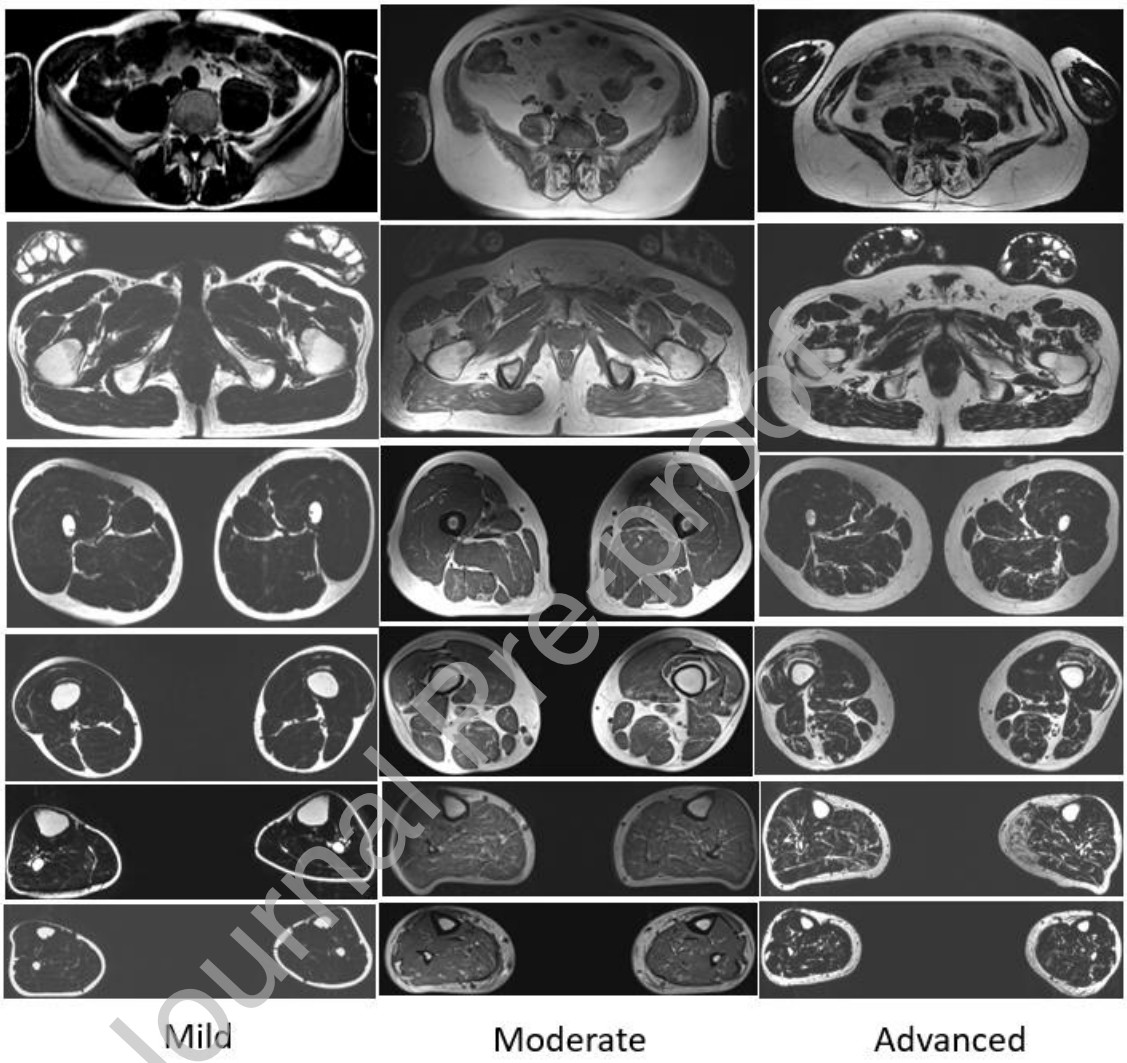

Fig 6 – Axial fat image of the DIXON technique sections exploring the different stages of findings in different disease stages of McArdle patients. The first one showed mild involvement, the second is more involved with fatty substitution of both quadratus femori (arrows), and the last one is more advanced with changing in the right quadratus femori and in the calf (arrow).

Table 1. Clinical and genetic characteristics of the 15 patients with McArdle disease. † nonsense mutation; ‡ missense mutation; * frameshift mutation; þ splicing)
New mutations are in bold type
Medical Research Council (MRC)

	Sex	Age	MRC scale rating for fixed muscle weakness	Genetic format	
Patient 1	M	55	Abduction 4 ; psoas 4	c.148C>T	c.148C>T
Patient 2	M	37	neck flexor 3/5 ; scapular winging	c.507G>T	c.507G>T
Patient 3	M	55	neck flexor 4	c.148C>T	c.1190C>T
Patient 4	F	39	none	c.148C>T	
Patient 5	M	84	abdominal muscles 3 ; neck flexor 3	c.148C>T	c.2353C>T
Patient 6	M	24	scapular winging	c.148C>T	c.148C>T
Patient 7	F	62	upper left limb 4 ; gluteal 4	c.148C>T	c.148C>T
Patient 8	M	50	neck flexor 4	c.148C>T	c.148C>T
Patient 9	F	35	neck flexor 4	c.148C>T	c.415C>T
Patient 10	M	44	scapular winging ; abduction 4	c.148C>T	c.1768+1G>A
Patient 11	M	61	neck flexor 4	c.148C>T	c.148C>T
Patient 12	M	47	none	c.148C>T	c.2262delA
Patient 13		47	scapular belt 4 ; abduction 4	c.613G>A	c.1475G>A
Patient 14	M	61	neck flexor 3 ; abduction 4 ; biceps 4 ; abdominal belt 4	c.148C>T	c.1615G>A
Patient 15	F	39	scapular winging, supra spinatus 4	c.148C>T	c.2056G>C